Computer Aided Diagnosis System using Watershed Segmentation with Xception Based Classification Model for Lung CT Images

D. Jayaraj, S. Sathiamoorthy

Abstract: *Early recognition and classification of pulmonary nodules by the use of computer-aided diagnosis (CAD) tools finds useful to reduce the death rate due to the illness of lung cancer. This paper devises a new CAD tool utilizing a segmentation based classification process for lung CT images. Initially, the input CT images are pre-processed by image enhancement and noise removal process. Then, watershed segmentation model is employed for the segmentation of the pre-processed images. Subsequently, the feature extraction process is carried out using Xecption model and random forest (RF) classifier is used of the identification of lung CT images as normal, benign or malignant. The use of RF model results to effective classification of the applied images. This model undergoes extensive experimentation against a benchmark lung CT image dataset and the results are investigated under several aspects. The obtained outcome pointed out the significant performance of the presented model over the compared methods.*

Index Terms: *CT image; Lung cancer; Classification; Random forest; Xception.*

I. INTRODUCTION

Lung cancer is considered to be most severe and similar disease throughout the world, where the rate increases for death as well as people who are vulnerable to this disease. In 2015, the survey states that one third of peoples are affected by lung cancer [1]. Also in 2017 US has secured the count of 225,000 for novel cases of lung cancer as well as 155,870 deaths are listed, 26% total number of cancer-related deaths occur accordingly [1]. Torre et al. [2], an amount of 55% of people's lifetime could be increased by detecting the lung cancer at early stage. By detecting the disease in early stage, if any lumps identified in lungs can be examined and treated accordingly.

Lung cancer is deducted utilizing Computed tomography (CT) which is most efficient technology in medicinal field that has the capability to build the 3D images of the upper body, gives the high dimension of nodule and tumor pathology.

Detecting lung cancer in early stage is not a simple task which consumes time: technicians have to analyze very carefully the lumps present in lungs using several images in CT scan. Doi [3] represents that radiologists might leave about 30% of lung nodules since it is overlapped among them and related general normal anatomic structure.

Computer-aided diagnosis (CAD) is a process that is developed, to help the medical officers and radiologists to detect the lump present in lungs. CAD finds useful for predicting the lung cancer. The pipeline of a CAD model is demonstrated in Fig. 1 [4]. According to its development, accurateness of lung cancer categorization is essential for the accomplishment of a CAD model.

Today, deep learning (DL) is a concept that is considered to be the optimal solutions for several issues of the system vision and pattern analysis. Convolution Neural Network (CNN), is a kind of neural network utilizes the convolution operators in its layer, that is applied commonly in detecting the object as well as classifying the outcome with respect to accurateness. This benefit of DL builds the ability to detect the lung nodule and classify the system.

CNN was developed from the basis of artificial neural network through convolution operators for achieving improved input image. This structural design is developed on the basis of biological visual system as well as it is highly efficient for image recognition issues, despite of sizes or scales. In this type of model, every neuron is connected to other one in a way such that it responds to the accessible region surrounding it. In addition, all neurons are linked to many "close by" other neurons, and then the quantity of weight for a CNN is very low when compared to a Fully Connected (FC) network. Hence, CNN generates extended accurateness to recognize the image and less amount of time is consumed while training the FC network. As inception [6], CNN is "deepen" with more projected networking models. For instance, AlexNet [7] consist of 8 layers with 1000 classes; VGG [8] has 25 layers as well as ResNet [9] holds a maximum of 152 layers.

Developing the compensation of DL, more number of techniques has been proposed to maximize classifying accurateness of lung nodule. [10] projected a 2D CNN to divide the nodules as cancer or normal. The presented model undergone the process of training and validation on LIDC/IDRI database.

Retrieval Number: A4618119119/2019©BEIESP
DOI: 10.35940/ijitee.A4618.119119
Journal Website: www.ijitee.org

3625

Published By:
Blue Eyes Intelligence Engineering
& Sciences Publication

Experimentally, this technique has the ability to increase the performance on lung nodule classification.

[11] projected a system aided technique to classify the lung cancer present in CT images. The classification process comprises of the statistical features namely mean, standard deviation, skewness, and so on. The feed forward back propagation neural network obtains an efficient classifier outcome compared to feed forward neural network. The research exhibited that it offered manageable results while analyzing the non-cancerous nodule in the approved manner.

[12] launched a pulmonary nodule detecting technique with the help of hierarchical block classification. This model splits the image into 3D blocks. Entropy analysis is a scheme that is used for choosing informative blocks to identify the nodule candidates. At last, support vector machine (SVM) is utilized to divide the nodules. The assessment on the LIDC database represents that this technique has the ability to obtain a great classification outcome.
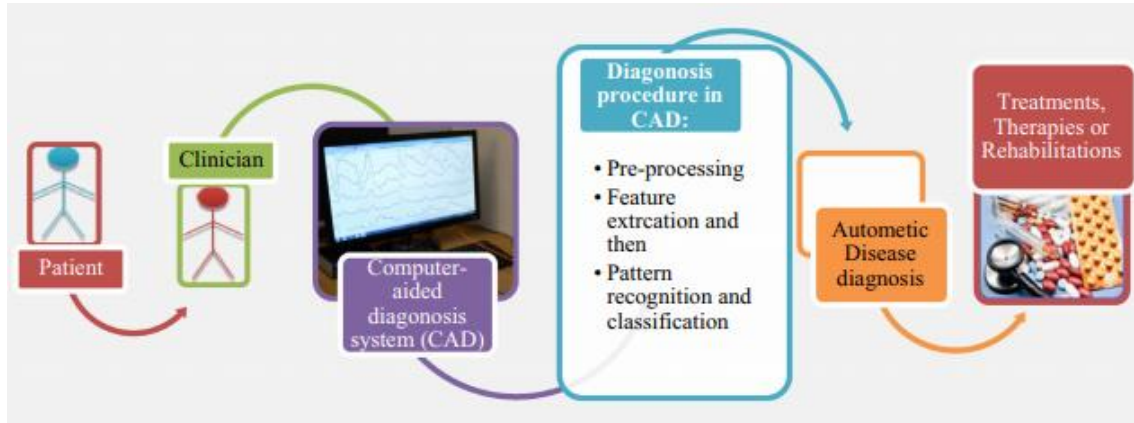

Fig. 1. Pipeline of CAD tool in medical image diagnosis

[13] used multitier convolutional networks (ConvNets) to find the affected area of lungs. This technique is helpful in training the count of 1,186 nodule filtered from LIDC/IDRI LUNA16 dataset. Practically it represents that it achieves around 90% of sensitivity. [14] utilized a network called Feed Forward Neural Network (FFNN) to classify the nodule candidates. The network pattern comprises of 13 input neurons, 1 hidden layer with 25 neurons, as well as 1 neuron present in the output layer to propose the binary classifier. The training as well as testing candidates was operated on 1,018 CT scans from the LIDC/IDRI dataset. As a result, the technique attains the sensitivity up to 89.1%. The LUNA16 challenge [15] projected an assessment model on automated nodule recognition technique with the help of commonly accessible reference database of CT scans [16]. The challenge filtered 1,186 lung nodules from LIDC-IDRI chest CT images as well as offered these nodules as optimistic applicant for researcher people. The result of this challenge illustrates that a best individual recognition model could reach up maximum results.

This paper devises a new CAD tool utilizing a segmentation based classification process for lung CT images. Initially, the input CT images are pre-processed by image enhancement and noise removal process. Then, watershed segmentation model is employed to segment the segmentation of the pre-processed images. Subsequently, the feature extraction process is carried out using Xecption model and random forest (RF) classifier is used of the identification of lung CT images as normal, benign or malignant. The use of RF model results to effective classification of the applied images. This model undergoes extensive experimentation against a benchmark lung CT image dataset and the results are investigated under several aspects. The obtained outcome pointed out the significant performance of the presented model over the compared methods.

The rest of the parts are organized here. Section 2 briefs the processes included in the presented model. Section 3 investigates the effectiveness of the presented work on the benchmark dataset and Section 4 concludes the work.

II. PROPOSED MODEL

The complete operational procedure is demonstrated in Fig. 2. At the initial stage, the images are pre-processed image to progress the quality and eliminate the noise present in the image. Next, image segmentation takes place utilizing the watershed algorithm. Then, a DL based Xception model is applied for prominent feature extraction and the classification takes place by the use of RF classification model. The effectiveness of the RF classifier represents whether the input CT lung image has cancer or not.

A. Pre-processing

In this paper, the pre-processing operates in two stages namely image enhancing and noise removal. Toward the start, AHE model is used due to effectiveness and low complexity. It enhances the image quality and visual effect by enlarging the distribution of grayscale values present in the image. It basically relies on the probability distribution function. It settles the troubles present in customary models through the automated discovery and versatile nature to the grayscale images.
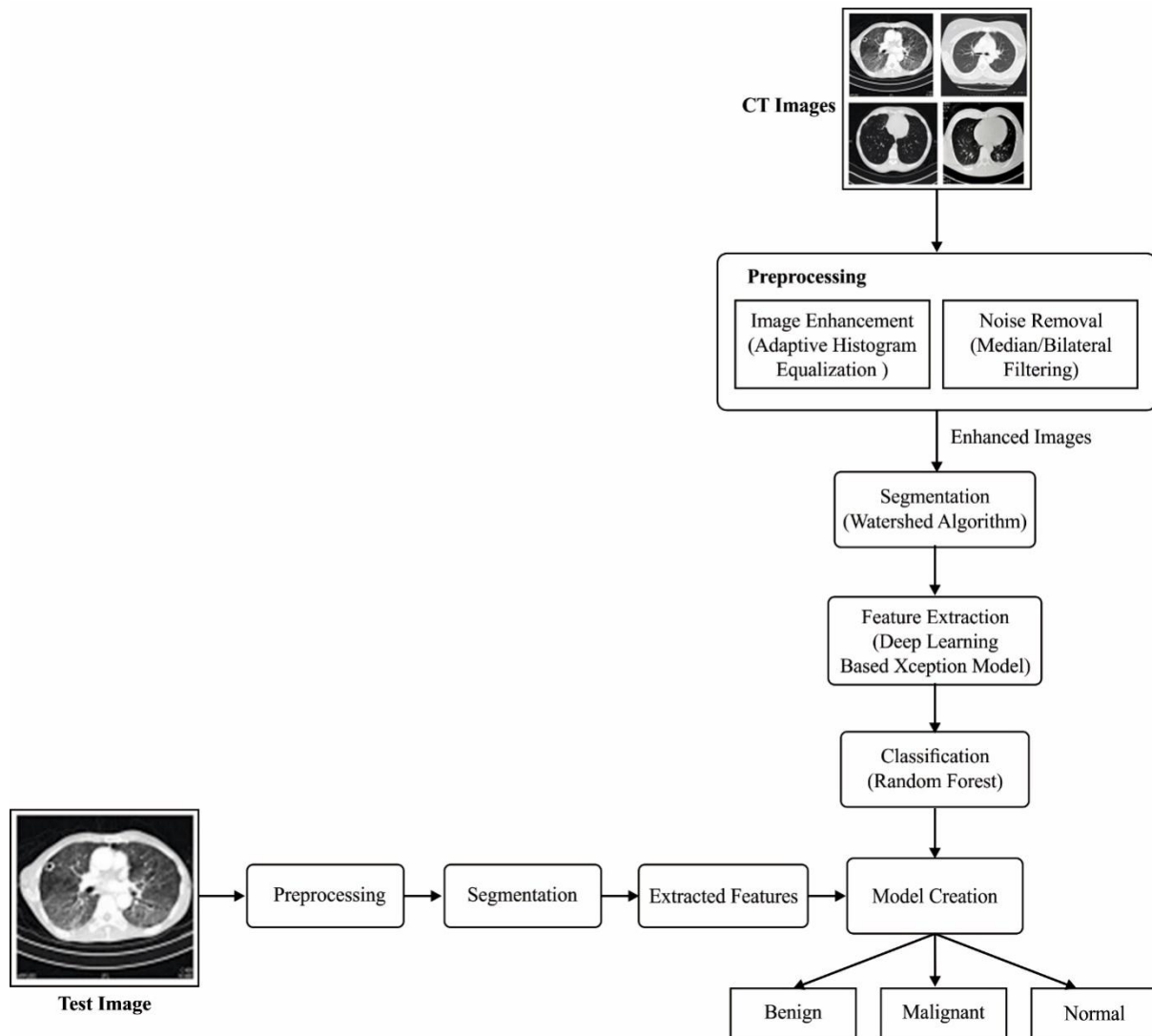
Fig. 2. Working procedure of presented model

At the subsequent level, BF is utilized on the CT images in grayscale structure. Typically, few measures of noises present in the CT image generation which may result in false identification of cancer nodules. Along these lines, it is expected to viably distinguish the noise before classification. The possibility of BF relies on a particular weighting component for averaging adjoining pixels for expelling the noises. The common way of representing BF comprises a distance based domain filter part (i, i'), and a gray-value dependent range filter part $r((f\,i),(f\,i'))$:

$$\tilde{f}(i) = \frac{1}{N(x)} \int_{-\infty}^{\infty} f(i')d(i,i')r(f(i),f(i'))di' \qquad (1)$$

Where i and i' denotes the location of the middle and adjacent pixels, and $N(i)$ a normalization factor. Once the domain filter assumes a local average of neighbouring pixels, the range filter part forces the value based element for eliminating the filter among the edges. For domain and range filter regions, generally, a Gaussian function is applied and is depends upon the Euclidean pixel distance as represented by

$$d(i,i') \propto \exp\left(-\frac{(i-i')^2}{2\sigma_d^2}\right) \qquad (2)$$

$$r(f(x),f(x')) \propto exp\left(-\frac{(f(x)-f(x'))^2}{2\sigma_f^2}\right) \qquad (3)$$

with σ_d is a width parameter of the filter kernel size and σ_f the noise standard deviation of the assumed reconstruction value (e.g. attenuation noise standard deviation σ_a)

Median filter is a nonlinear statistical filter which replaces the present pixel values with the median value of pixels present in the nearby area. A naive implementation initially generates a cumulative histogram for the neighbouring area and also determines the initial index beyond half the number of pixels in the histogram.

B. Watershed based image segmentation

This system expects a figure as a topographic scene with edges just as valleys. The altitude value of the scene is generally seen by the gray values of the specific pixels or the gradient magnitudes. With respect to the 3D representation of the watershed transform, images are decomposed using a collection of catchment basins. In every local minima, it contains the root whose course of steepest drop end at the minima is displayed in Fig. 3. The watershed transform operation gives the whole image partitioning just as distributing every pixel to a segment or watershed. Concerning noisy healthcare images, maximum number of tiny portions is considered as an issue of over segmentation. On the off chance that image segmentation is to be performed, feature extracting procedure is indispensable.
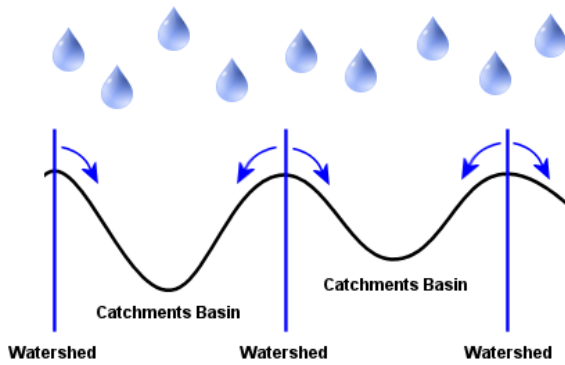

Fig. 3. Watershed transform

For effective extraction of features, it is critical to gather the voxel wise morphometric features to regional features which hold high dimensional features including massive number of duplicate or unwanted data and noise because of existing error in registration procedure. In an identical way, using the provincial features can minimize this issue just as to give more beneficial features in the classifier procedure. A traditional method to accomplish the local features is to use previous information, for example fixed ROI that audit each voxel wise features in each fixed ROI. In any case, it was not efficient while use of a few layouts to symbolize CT images, as the ROI features from different formats is progressively normal. To catch various kinds of different CT image features from different layouts, a clustering technique is applied for dynamic gathering of features. It reveals that the usage of clustering model enhance the discriminative intensity of the attained regional features, and decrease the unhelpful contact from the registration error.

Let $I_i^j(v)$ signifies a voxel-wise cell thickness value at voxel u in the kth format for the ith training subject, $i \in [1, N]$. The ROI part for the kth template depends on the consolidated separation and robustness metric, $DRM^j(v)$, concluded from all the N preparing subjects that expect the feature importance and spatial reliability quality into account. It can be indicated as

$$DRM^j(v) = P^j(v)C^j(v) \qquad (4)$$

where $P^j(v)$ is the voxel-wise Pearson relationship (PC) from all individual N preparing subjects, and $C^j(v)$ demonstrates the spatial steadiness between each feature in the spatial neighbourhood. Watershed segmentation is prepared on each

processed DRM^j map to accomplish the ROI area for the kth template. In noticing the Gaussian kernel is utilized for smoothing all maps DRM^j to eliminate over segmentation. Accordingly, the kth layout could be splitted to a complete R^j non covering regions; it ought to be seen that all format provides an output under individual ROI area.

C. Xception model based feature extraction

Xception model is designed by Chollet, who developed the Keras library. It is an extended model of Inception which undergoes a replacement with the conservative Inception module using depth-wise separable convolution. The structure of CNN is basically founded on depth-wise distinct conv layers that is offered. The set of following assumption planned that match the cross-channels just as spatial connection in the element maps of CNN that is entirely decoupled. On account of this reality, an effective hypothesis is introduced utilizing essential Inception design, the proposed Xception strategy signifies "Extreme Inception" and comparing units are clear which is portrayed in Fig. 4. The Xception model involves 36 convolutional layers that build the element extracting base of the system. In simulation part, image classification is completed by exploring just as convolutional base is logistic regression layer. It is not necessary that the totally associated layers ought to be incorporated at the previous stage to the logistic regression layer. There are 36 convolutional layers which are organized into 14 parts, every unit comprise of linear connections around them leaving the underlying and last modules. In short, the Xception design has a linear stack of depth wise independent conv layers with remaining connections. These features are useful as far as simple description just as for alteration. It requires just less number of coding that is from the high level library like Keras or TensorFlow-Slim, distinctly to the models, for example, VGG-16, yet the open Inception V2 or V3 methods are not all that simple to portray.

Xception comes from the Inception model which undergoes replacement by the use of depth wise separable convolutions. It has around identical parameter count as Inception-v1 model. The convolution and pooling operations are employed for automated feature extraction and reduction. Consider an image X of size (i, j), the representation of convolution takes place as follows.

$$C(i,j) = (I * w)(i,j) = \sum_k \sum_l I(i-k, j-l)w(k,l) \qquad (5)$$

where w is the convolution kernel size of (k, l). The convolution offers a way of learning the images and the parameter sharing reduces the model complexity. Pooling acts as a procedure of dropping the features. It assumes a set of close by pixels in the feature map and generates a value for representation. The feature map is characterized as 4×4, the maximum pooling makes a greatest incentive in every 2×2 square that limits the feature measurement extensively.

Cross channel standardization goes under a neighborhood standardization model that upgrades the generalization. The feature maps experience standardization in preceding feed to the next layers. The cross channel standardization gives a whole from assorted contiguous maps at the indistinguishable area. This procedure can be found in real neurons.
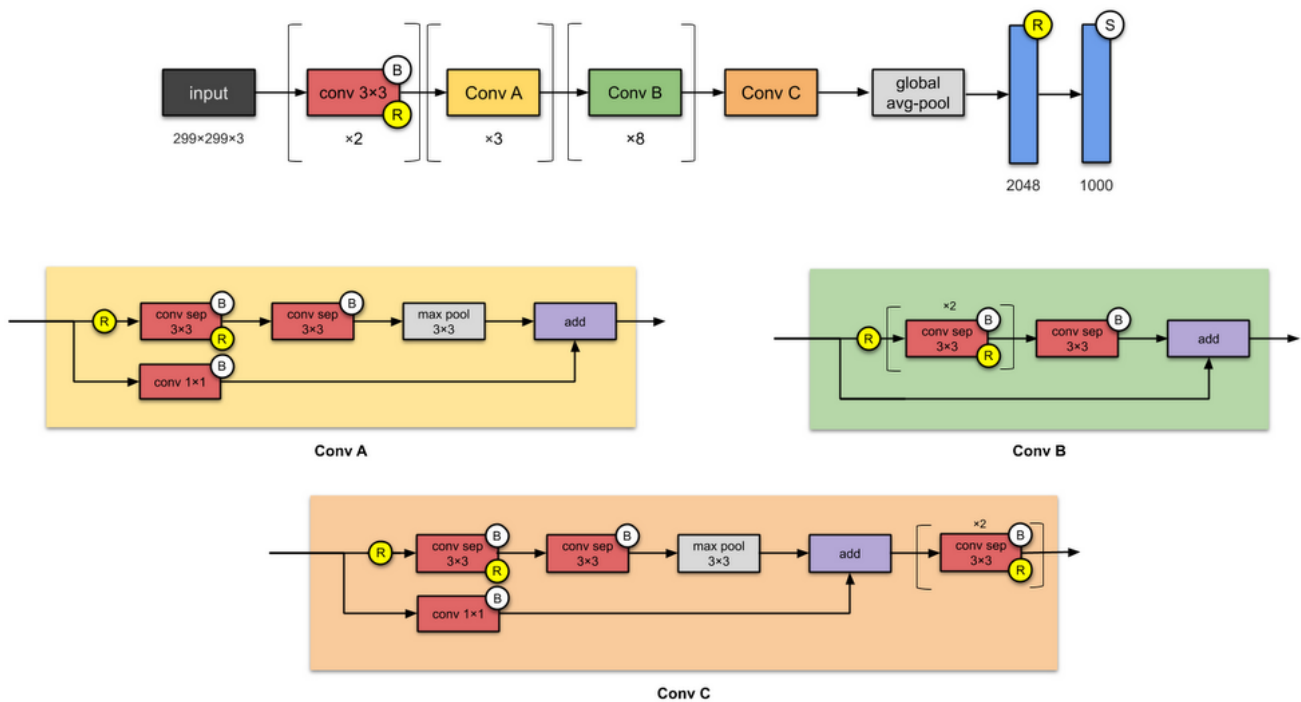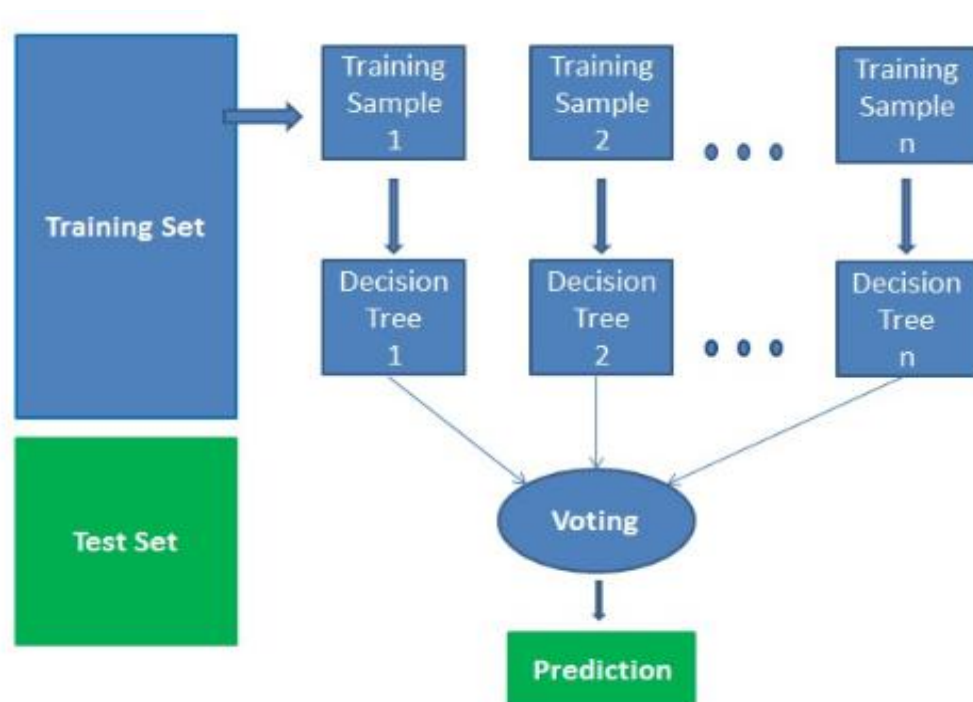

Fig. 4. Xception architecture

Fig. 5. RF classifier

D. RF based classification

Random forest (RF) model can be employed to classify the images promptly. It indicates adaptability and holds a lot of trees. It is characterized that progressively number of trees makes it powerful. RF creates the DT on the self-assertively picked data tests, performs expectation from each tree and picks the ideal arrangement through voting. It offers a productive pointer to tell the essentialness of highlights. RF is utilized in assorted applications namely proposal motors, picture classification and highlight choice.

This investigation utilizes RF classifier to recognize the classification the lung CT images. It is commonly an ensemble strategy extending upon the technique for divide and conquer technique. It has a lot of DTs based on a randomly partitioned dataset as appeared in Fig. 5. This arrangement of DT classifiers is likewise called as a forest. A gathering of independent DTs is produced using attribute choice pointer like gain ration, and Gini index for each factor. Each individual tree depends on a free subjective example. To classify the data, each tree will cast a ballot and the commonplace class is chosen as the end result.

III. EXPERIMENTAL VALIDATION

This paper employs a benchmark lung cancer CT image dataset consists of a group of fifty low-dosage images [17] which are generally in 1.25mm slice thick. It is generally acquired through a single inhale as well as exhale. The location of the cancer nodules are recognized by the professionals which are also provided in the dataset. This information is available in Table 1 and the sample test images are demonstrated in Fig. 6. It is observed that a sum of 900 images exist where a total of 300 images comes under each level of 0, 1 and 2 correspondingly.

Table 1 Dataset Description

Description	Lung Database
Class count	3
Benign/Malignant/Normal	Label (0/1/2)
Benign image count	300
Malignant image count	300
Normal image count	300
Total image count	900

A. Evaluation parameters

Three measures are employed for the experimentation are sensitivity, specificity, accuracy, positive predictive value (PPV) and negative predictive value (NPV).
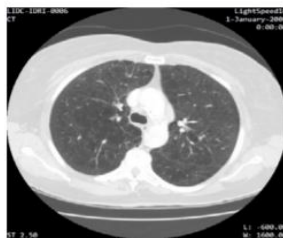
$$Sensitivity = \frac{TP}{TP + FN} \tag{8}$$
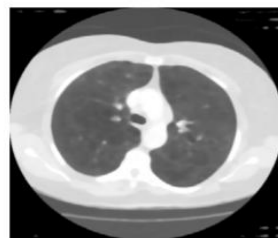
$$Specificity = \frac{TN}{TN + FP} \tag{9}$$

$$Accuracy = \frac{TP + TN}{TP + FP + FN + TN} \tag{10}$$

$$PPV = \frac{TP}{TP + FP} \tag{11}$$

$$NPV = \frac{TN}{TN + FN} \tag{12}$$

where TP, TN, FP and FN indicate true positive, true negative, false positive and false negative in that order.
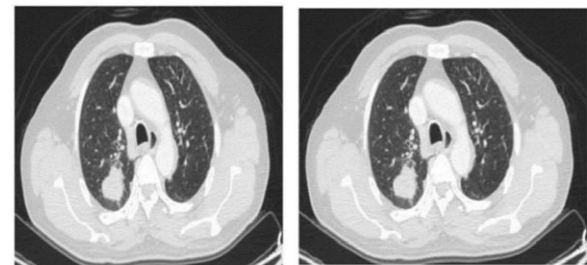

Fig. 6. Sample test images

B. Results analysis

Fig. 7 illustrates the images generated using the pre-processing level. Fig. 7b illustrates the image obtained by the applied AHE model for enhancing the image contrast. At the same time, the original image and the corresponding noise removed images using bilateral and median filtering are shown in Fig. 8. From this figure, it is evident that the image generated by the bilateral filtering is better than the median filtering images.

Table 2 provided the classification outcome by the RF model under different classes. The second row clearly indicated that the presented model precisely classifies the benign image as benign. Next, the third row obviously defines that the presented model accurately classifies the malignant image as malignant. The final row evidently denotes that the presented model precisely classifies the normal image as normal.
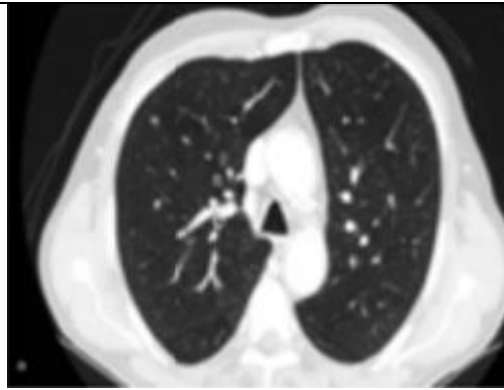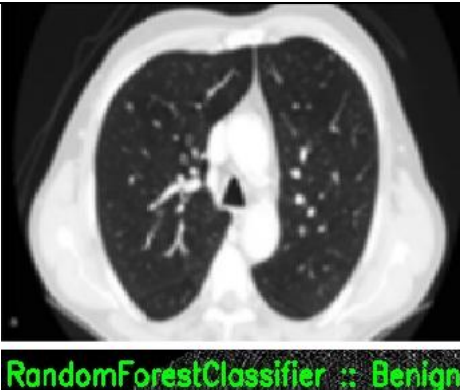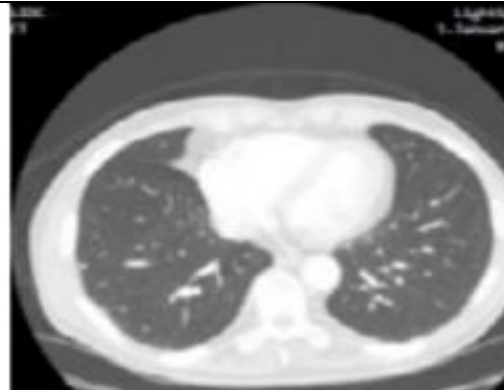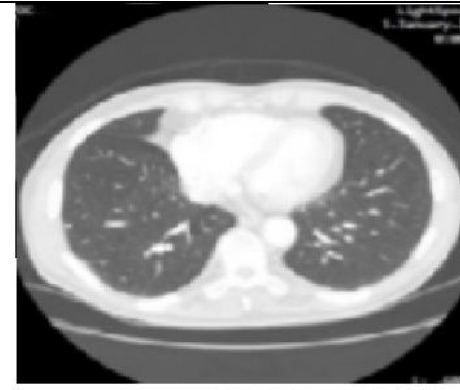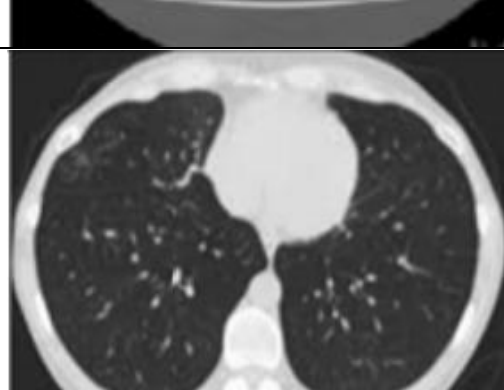

(a)   (b)

Fig. 7. (a) Original Image (b) AHE image

(a)   (b)   (c)

Fig. 8. (a) Original Image (b) Bilateral Filtering (c) Median Filtering

Table 2 Visualization of classifier results

Classes	Original Image	Classified Image
Benign		
Malignant		
Normal		
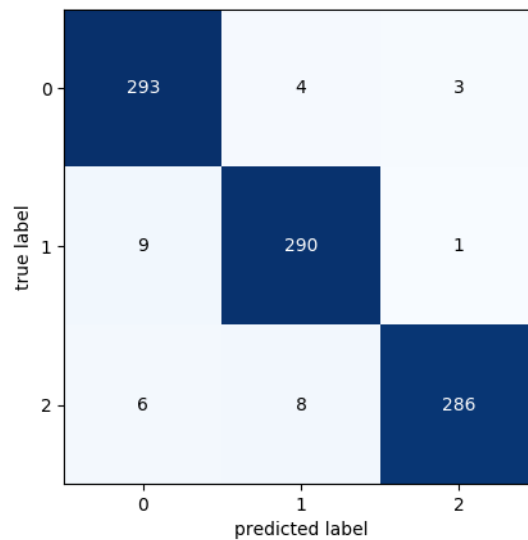
Fig. 9. Confusion matrix

Fig. 9 demonstrated the obtained confusion matrix from classifier model. Among the total of 900 images, the presented model clearly classifies 293 images as benign, 290 images as malignant and 286 images as normal. The confusion matrix is derived in Table 4.

For determining the goodness of the provided RF model, the generated 4×4 matrix undergo transformation to 2×2 matrix as given in Table 4.

Table 3 Derived Confusion Matrix

Input Label	Different Classes in Lung Cancer			Image count
	Benign	Malignant	Normal	
Benign	293	4	3	300
Malignant	9	290	1	300
Normal	6	8	286	300
Image count	308	302	290	900

Table 4 Manipulations from Confusion Matrix

Classes	Benign	Malignant	Normal
TP	293	290	286
TN	576	579	583
FP	15	12	4
FN	7	10	14

Table 5 Classifier results analysis under three classes

Classes	Sensitivity	Specificity	Accuracy	PPV	NPV
Benign	97.67	97.46	97.53	95.13	98.80
Malignant	96.67	97.97	97.53	96.03	98.30
Normal	95.33	99.32	97.97	98.62	97.65

Table 5 and Fig. 10 display the results attained by the projected model interms of different measures. As shown, it is noted that the benign CT lung images are effectively classified with the sensitivity of 97.67, specificity of 97.46, accuracy of 97.53, PPV of 95.13 and NPV of 98.80. At the same time, it is observed that the malignant CT lung images are effectively classified with the sensitivity of 96.67, specificity of 97.97, accuracy of 97.53, PPV of 96.03 and NPV of 98.30. In the same way, the normal images are effectively classified with the sensitivity of 95.33, specificity of 99.32, accuracy of 97.97, PPV of 98.62 and NPV of 97.65. These values exhibited that the presented model shows effective classified under the normal CT lung images.

Table 6 offered the comparative analysis of existing models with the presented one with respect to diverse measures. In addition, to clearly understand the betterment of the presented model, Figs. 11-13 visualize the comparative results of diverse models with respect to accuracy, sensitivity and specificity respectively.
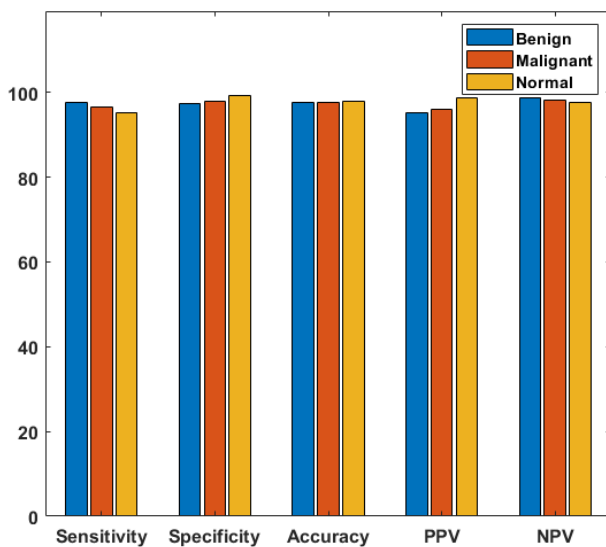

Fig. 10. Classifier results analysis under several measures

Table 6 Comparative analysis of various methods in terms of Accuracy, Sensitivity and Specificity

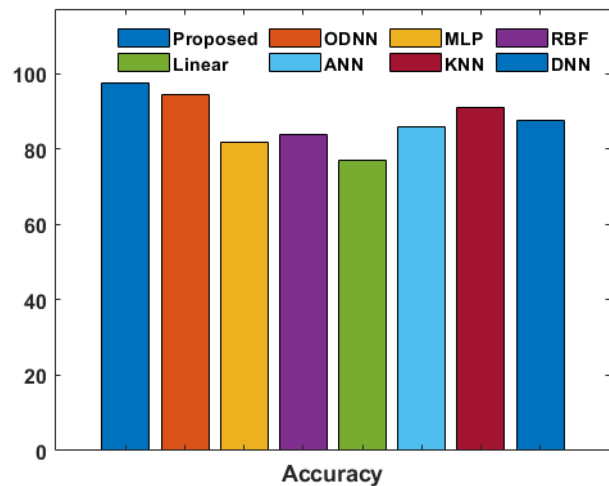| Methods	Accuracy	Sensitivity	Specificity
Proposed	97.68	96.56	98.25
ODNN	94.56	96.20	94.20
MLP	82.00	77.00	72.00
RBF	84.00	86.00	54.00
Linear	77.00	89.00	36.00
ANN	86.00	87.00	79.00
KNN	91.00	90.00	83.00
DNN	87.65	82.43	89.67

Fig. 11. Accuracy analysis of various models

Fig. 11 demonstrates the accuracy investigation of differing models on the classification of lung CT images. It tends to be seen that the linear regression model shows ineffectual classification by accomplishing an accuracy of 77. In like manner, the MLP classifier model achieves moderate classification with the accuracy of 82. Similarly, the RBF model accomplishes marginally higher classification with accuracy of 84. Similarly, the ANN model gets better classification accuracy of 86 over different models. In accordance with, the DNN model attempted to oversee well with the accuracy of 87.63. Next, the ODNN model display focused classification over the presented model by accomplishing the higher accuracy estimation of 94.56. Be that as it may, most extreme classification execution is accomplished by presented model with the accuracy of 97.68.

Fig. 12 demonstrates the sensitivity investigation of various models on the classification of lung CT images. It very well may be seen that the MLP model shows inadequate classification by accomplishing a base sensitivity of 77. Simultaneously, the DNN classifier model accomplishes moderate classification with the sensitivity of 82.43. Similarly, the RBF model accomplishes somewhat higher classification with sensitivity of 86.
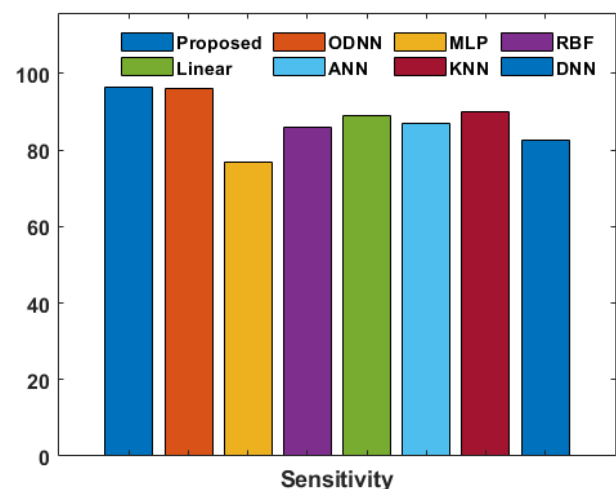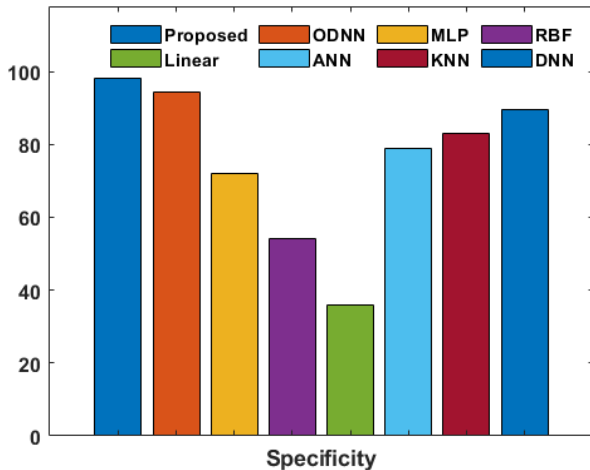

Fig. 12. Sensitivity analysis of various models

In like manner, the ANN model gets better classification sensitivity of 87 over different models. In accordance with, the straight relapse model attempted to oversee well with the sensitivity of 89. Next, the ODNN model show focused classification over the presented model by accomplishing the higher sensitivity estimation of 96.30. In any case, most extreme classification execution is accomplished by presented model with the sensitivity of 96.56.


Fig. 13. Specificity analysis of various models

Fig. 13 demonstrates the specificity investigation of different models on the classification of lung CT images. It tends to be seen that the linear regression model shows inadequate classification by achieving a specificity of 36.

Simultaneously, the RBF classifier model accomplishes moderate classification with the specificity of 54. Similarly, the MLP model accomplishes somewhat higher classification with the specificity of 72. Similarly, the ANN model gets better classification specificity of 79 over different models. In accordance with, KNN model attempted to oversee well with the specificity of 83. Next, the ODNN model show focused classification over the presented model by accomplishing the higher specificity estimation of 94.20. Be that as it may, greatest classification execution is achieved by presented model with the specificity of 98.25.

Fig. 14 shows the further effectiveness of the projected model interms of ROC. From the figure, it is noticed that maximum classification is attained by the projected model with the ROC value of 96.85. By investigating the above tables and figures, it is evident that exceptional classification of lung CT images is shown by the presented model by accomplishing the most extreme accuracy of 97.68, sensitivity of 96.56 and specificity of 98.25 separately. These improved results pointed out that it tends to be utilized to test ongoing CT lung images.
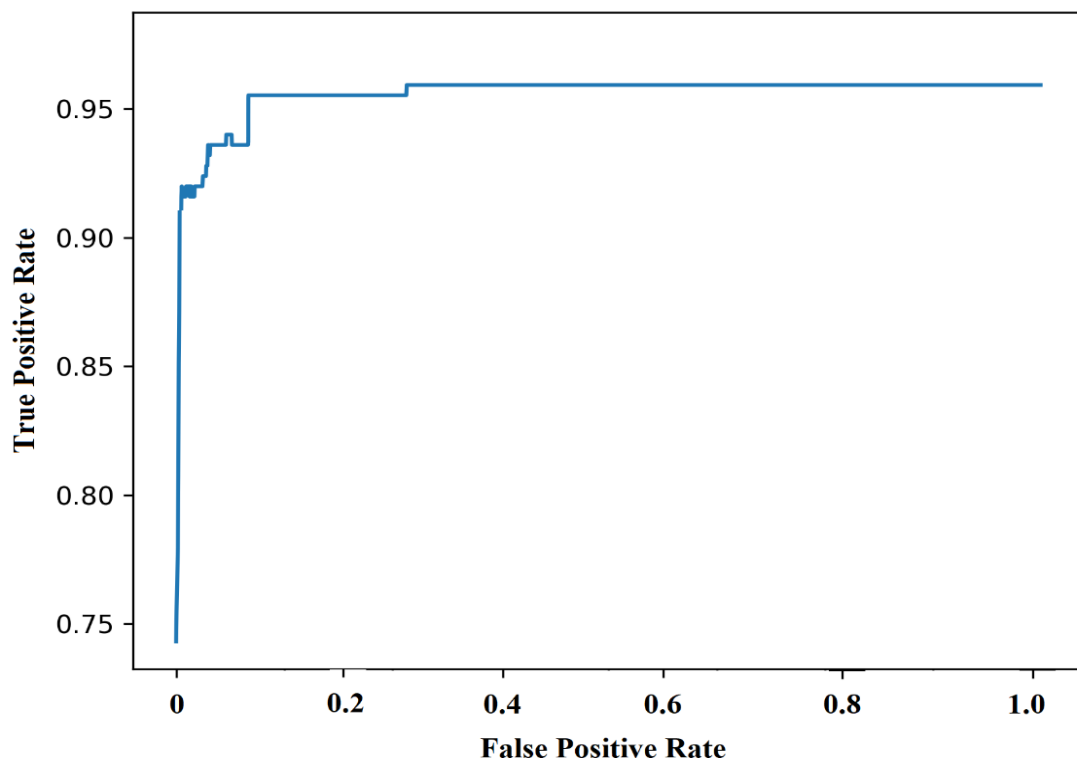
Fig. 14. ROC analysis

IV. CONCLUSION

This paper has presented a new CAD tool utilizing a segmentation based classification process for lung CT images. Initially, the input CT images are pre-processed by image enhancement and noise removal process. Then, watershed segmentation model is applied for the segmentation of the pre-processed images. Subsequently, the feature extraction process is carried out using Xecption model and RF classifier is used of the identification of lung CT images as normal, benign or malignant. The use of RF model results to effective classification of the applied images. This model undergoes extensive experimentation against a benchmark lung CT image dataset most extreme accuracy of 97.68, sensitivity of 96.56 and specificity of 98.25 separately. These improved results pointed out that it tends to be utilized to test ongoing CT lung images. As a part of future scope, image clustering techniques can be incorporated as a part of diagnosis process.

REFERENCES

1. R. L. Siegel, K. D. Miller, and A. Jemal, "Cancer statistics, 2017," CA: A Cancer Journal for Clinicians, vol. 67, no. 1, pp. 7–30, 2017
2. L. A. Torre, R. L. Siegel, and A. Jemal, "Lung cancer statistics," in Lung Cancer and Personalized Medicine, pp. 1–19, Springer, Berlin, Germany, 2016
3. K. Doi, "Computer-aided diagnosis in medical imaging: historical review, current status and future potential," Computerized Medical Imaging and Graphics, vol. 31, no. 4-5, pp. 198–211, 2007.
4. Q. Song, L. Zhao, X. Luo, and X. Dou, "Using deep learning for classification of lung nodules on computed tomography images," Journal of Healthcare Engineering, vol. 2017, Article ID 8314740, 7 pages, 2017
5. T.-Y. Lin, P. Goyal, R. Girshick, K. He, and P. Dollar, "Focal ´loss for dense object detection," in Proceedings of 2017 IEEE International Conference on Computer Vision (ICCV), pp. 2999–3007, Venice, Italy, October 2017.
6. Y. Lecun, L. Bottou, Y. Bengio, and P. Haffner, "Gradientbased learning applied to document recognition," in Proceedings of the IEEE, vol. 86, no. 11, pp. 2278–2324, 1998
7. A.Krizhevsky, I. Sutskever, and G. E. Hinton, "ImageNet classification with deep convolutional neural networks," in Proceedings of the 25th International Conference on Neural Information Processing Systems-Volume 1, NIPS'12, pp. 1097–1105, Curran Associates Inc., Lake Tahoe, NV, USA, December 2012.
8. K. Simonyan and A. Zisserman, "Very deep convolutional networks for large-scale image recognition," in Proceedings of IEEE International Conference on Learning Representations, Banff, AB, Canada, April 2014.
9. K. He, X. Zhang, S. Ren, and J. Sun, "Deep residual learning for image recognition," in Proceedings of 2016 IEEE Conference on Computer Vision and Pattern Recognition (CVPR), pp. 770–778, Las Vegas, NV, USA, June 2016.
10. W. Li, P. Cao, D. Zhao, and J. Wang, "Pulmonary nodule classification with deep convolutional neural networks on computed tomography images," Computational and Mathematical Methods in Medicine, vol. 2016, Article ID 6215085, 7 pages, 2016.
11. J. Kuruvilla and K. Gunavathi, "Lung cancer classification using neural networks for CTimages," Computer Methods and Programs in Biomedicine, vol. 113, no. 1, pp. 202–209, 2014.
12. W.-J. Choi and T.-S. Choi, "Automated pulmonary nodule detection system in computed tomography images: a hierarchical block classification approach," Entropy, vol. 15, no. 2, pp. 507–523, 2013
13. A. A. A. Setio, F. Ciompi, G. Litjens et al., "Pulmonary nodule detection in CT images: false positive reduction using multiview convolutional networks," IEEE Transactions on Medical Imaging, vol. 35, no. 5, pp. 1160–1169, 2016.
14. E. L. Torres, E. Fiorina, F. Pennazio et al., "Large scale validation of the M5L lung CAD on heterogeneous CT datasets," Medical Physics, vol. 42, no. 4, pp. 1477–1489, 2015.
15. A. A. A. Setio, A. Traverso, T. de Bel et al., "Validation, comparison, and combination of algorithms for automatic detection of pulmonary nodules in computed tomography images: the LUNA16 challenge," Medical Image Analysis , vol. 42, pp. 1–13, 2017.
16. S. G. Armato III, G. McLennan, L. Bidaut et al., "e lung image database consortium (LIDC) and image database resource initiative (IDRI): a completed reference database of lung nodules on ct scans," Medical Physics, vol. 38, no. 2, pp. 915–931, 2011.
17. http://www.via.cornell.edu/lungdb.html